INTERNATIONAL JOURNAL FOR NUMERICAL METHODS IN FLUIDS
Int. J. Numer. Meth. Fluids 2004; **44**:33–53 (DOI: 10.1002/fld.621)

A transformation-free HOC scheme for steady convection–diffusion on non-uniform grids

Jiten C. Kalita[1,*,†,‡], Anoop K. Dass[2,§,¶] and D. C. Dalal[3,‖,**]

[1]*Department of Mathematics, The George Washington University, Washington, DC 20052, U.S.A.*
[2]*Department of Mechanical Engineering, Indian Institute of Technology Guwahati, PIN 781039, India*
[3]*Department of Mathematics, Indian Institute of Technology Guwahati, PIN 781039, India*

SUMMARY

A higher order compact (HOC) finite difference solution procedure has been proposed for the steady two-dimensional (2D) convection–diffusion equation on non-uniform orthogonal Cartesian grids involving no transformation from the physical space to the computational space. Effectiveness of the method is seen from the fact that for the first time, an HOC algorithm on non-uniform grid has been extended to the Navier–Stokes (N–S) equations. Apart from avoiding usual computational complexities associated with conventional transformation techniques, the method produces very accurate solutions for difficult test cases. Besides including the good features of ordinary HOC schemes, the method has the advantage of better scale resolution with smaller number of grid points, with resultant saving of memory and CPU time. Gain in time however may not be proportional to the decrease in the number of grid points as grid non-uniformity imparts asymmetry to some of the associated matrices which otherwise would have been symmetric. The solution procedure is also highly robust as it computes complex flows such as that in the lid-driven square cavity at high Reynolds numbers (*Re*), for which no HOC results have so far been seen. Copyright © 2004 John Wiley & Sons, Ltd.

KEY WORDS: convection–diffusion; HOC; non-uniform; resolution; efficient; high-*Re*

1. INTRODUCTION

Finite difference method is frequently used in computational fluid dynamics. The method essentially consists in setting up a grid in the problem domain, discretizing the governing equations with respect to the grid and solving them numerically. The common practice is to

*Correspondence to: J. C. Kalita, Department of Mathematics, Indian Institute of Technology Guwahati, PIN 781039, India.
†Visiting Assistant Professor.
‡E-mail: G10@postmark.net
§Associate Professor.
¶E-mail: anoop@iitg.ernet.in
‖Associate Professor.
**E-mail: durga@iitg.ernet.in

Received 3 January 2002
Revised 20 June 2002

use a uniform grid, though it may not be the most appropriate one for efficient computation. Accurate resolution of the solution requires that grid points are clustered in the regions of large gradients while economy demands that they are spread out in the regions of small gradients [1–3]. Hence a non-uniform grid is indicated for many flow configurations. The popular approach is to map the physical space with a non-uniform grid onto a computational space with uniform grid where a transformed set of equations is first solved before mapping this solution back onto the physical space. Disadvantages of such an approach are many. There is a substantial increase in the number of terms to be discretized in the transformed governing equation giving rise to added computation. Many a time the transformation of the equations results in the appearance of cross-derivative terms which increases the computational complexity in many solution algorithms [3]. Moreover if the transformation is not explicitly known, it may have to be generated by numerical solution of some differential equation and this results in additional error. Overall, the solution procedure becomes complicated, expensive and sometimes error-prone.

The HOC finite difference schemes for the computation of incompressible viscous flows [4–13] are gradually gaining popularity because of their high accuracy and advantages associated with compact difference stencils. However such computations have so far been carried out only on uniform grids [4–9, 11–13]. In a departure from this practice, Spotz and Carey [14], and Zhang *et al.* [15] recently applied a fourth-order accurate HOC scheme on a non-uniform grid to linear convection–diffusion equations without source term. They use the conventional transformation technique which inevitably brings in the complications of having to deal with some new cross-derivative terms in the transformed partial differential equations (PDE) in addition to the increase in terms of arithmetic operations. Also, the advantage of setting the diffusive coefficients appearing in the PDEs in the physical space to unity is lost because they no longer remain the same in the transformed space. An additional constraint is that the transformation has to be carried out in such a way as to keep the grid aspect ratio unity in the computational space. In the present work, we propose an HOC scheme on rectangular non-uniform grids for the steady 2D convection–diffusion equation with variable coefficients without any transformation. It is based on the Taylor series expansion of a continuous function at a particular point for two different step lengths and approximation of the derivatives appearing in the 2D convection–diffusion equation on a non-uniform stencil. The original PDE is then used again to replace the derivative terms appearing in the finite difference approximations, resulting in a higher order scheme on a compact stencil of nine points. We have seen that the grid aspect ratio in the earlier HOC schemes has to be necessarily unity. Even in the case where non-uniform grid has been used with transformation [14, 15], this constraint remain in the computational space. The present scheme not only frees HOC schemes from such a constraint, but also makes it possible to use whatever non-uniform pattern of spacing one chooses in either direction. The order of accuracy of the scheme is four or three based on the pattern of grid spacing. Apart from avoiding the complexities associated with transformation techniques, this method affords a solution procedure that marries the virtues of a clustered grid to the efficiency of an HOC scheme. To validate the algorithm, the method has first been tested on two problems governed by linear PDEs for which analytical solutions exist. The power of the algorithm is better realized when applied to fluid flow problems governed by the 2D incompressible N–S equations at high *Re*'s in that it captures the physics of the flow accurately with relatively smaller number of grid points—a result of grid clustering—with complexities not higher than that associated with an HOC scheme on a uniform grid.

The scheme handles both Dirichlet and Neumann boundary conditions with ease and has the potential for extension to transient flow problems and curvilinear co-ordinates as well.

The paper is organized in four sections. Section 2 describes the basic formulations and numerical procedures, Section 3 the numerical results for three linear and non-linear test cases and Section 4 the conclusions.

2. BASIC FORMULATIONS AND NUMERICAL PROCEDURE

Consider a rectangular domain $a_1 \leqslant x \leqslant a_2$, $b_1 \leqslant y \leqslant b_2$. We divide the interval $[a_1, a_2]$ into sub-intervals, not necessarily of equal length, by the points $a_1 = x_0, x_1, x_2, \ldots, x_{m-1}, x_m = a_2$ and similarly $[b_1, b_2]$ by the points $b_1 = y_0, y_1, y_2, \ldots, y_{n-1}, y_n = b_2$. In the x-direction, the forward and backward step lengths are given by $x_\mathrm{f} = x_{i+1} - x_i$ and $x_\mathrm{b} = x_i - x_{i-1}$, respectively, and similarly, in the y-direction, we have $y_\mathrm{f} = y_{j+1} - y_j$ and $y_\mathrm{b} = y_j - y_{j-1}$, $1 \leqslant i \leqslant m-1$, $1 \leqslant j \leqslant n-1$. For a function $\Phi(x, y)$ assumed smooth in the given domain, a Taylor series expansion at point $(i+1, j)$ (Figure 1)

gives

$$\Phi_{i+1,j} = \Phi_{i,j} + x_\mathrm{f} \left.\frac{\partial \Phi}{\partial x}\right|_{ij} + \frac{x_\mathrm{f}^2}{2!} \left.\frac{\partial^2 \Phi}{\partial x^2}\right|_{ij} + \frac{x_\mathrm{f}^3}{3!} \left.\frac{\partial^3 \Phi}{\partial x^3}\right|_{ij} + \frac{x_\mathrm{f}^4}{4!} \left.\frac{\partial^4 \Phi}{\partial x^4}\right|_{ij} + \frac{x_\mathrm{f}^5}{5!} \left.\frac{\partial^5 \Phi}{\partial x^5}\right|_{ij} + O(x_\mathrm{f}^6) \tag{1}$$

Similarly at $(i-1, j)$

$$\Phi_{i-1,j} = \Phi_{i,j} - x_\mathrm{b} \left.\frac{\partial \Phi}{\partial x}\right|_{ij} + \frac{x_\mathrm{b}^2}{2!} \left.\frac{\partial^2 \Phi}{\partial x^2}\right|_{ij} - \frac{x_\mathrm{b}^3}{3!} \left.\frac{\partial^3 \Phi}{\partial x^3}\right|_{ij} + \frac{x_\mathrm{b}^4}{4!} \left.\frac{\partial^4 \Phi}{\partial x^4}\right|_{ij} - \frac{x_\mathrm{b}^5}{5!} \left.\frac{\partial^5 \Phi}{\partial x^5}\right|_{ij} + O(x_\mathrm{b}^6) \tag{2}$$

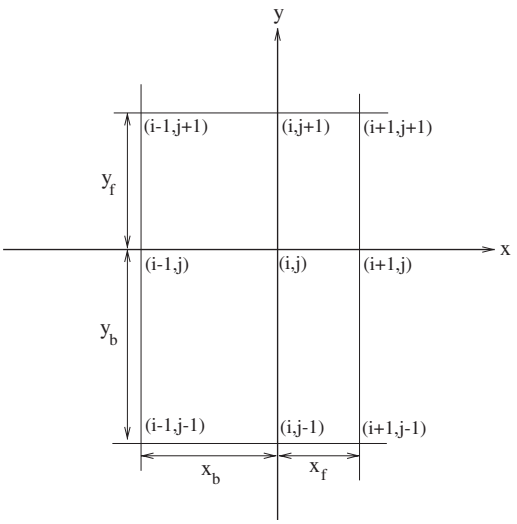

Figure 1. Non-uniform HOC stencil.

From Equations (1) and (2), we have

$$\left.\frac{\partial\Phi}{\partial x}\right|_{ij} = \frac{\Phi_{i+1,j}-\Phi_{i-1,j}}{x_\mathrm{f}+x_\mathrm{b}} - \frac{1}{2}(x_\mathrm{f}-x_\mathrm{b})\left.\frac{\partial^2\Phi}{\partial x^2}\right|_{ij} - \frac{1}{6}(x_\mathrm{f}^2+x_\mathrm{b}^2-x_\mathrm{f}x_\mathrm{b})\left.\frac{\partial^3\Phi}{\partial x^3}\right|_{ij}$$
$$-\frac{1}{4!}(x_\mathrm{f}-x_\mathrm{b})(x_\mathrm{f}^2+x_\mathrm{b}^2)\left.\frac{\partial^4\Phi}{\partial x^4}\right|_{ij} + O\left(\frac{x_\mathrm{f}^5+x_\mathrm{b}^5}{x_\mathrm{f}+x_\mathrm{b}}\right) \tag{3}$$

and

$$\left.\frac{\partial^2\Phi}{\partial x^2}\right|_{ij} = \frac{2}{(x_\mathrm{f}+x_\mathrm{b})}\left[\frac{\Phi_{i+1,j}}{x_\mathrm{f}}+\frac{\Phi_{i-1,j}}{x_\mathrm{b}}-\left(\frac{1}{x_\mathrm{f}}+\frac{1}{x_\mathrm{b}}\right)\Phi_{i,j}\right] - \frac{1}{3}(x_\mathrm{f}-x_\mathrm{b})\left.\frac{\partial^3\Phi}{\partial x^3}\right|_{ij}$$
$$-\frac{1}{12}(x_\mathrm{f}^2+x_\mathrm{b}^2-x_\mathrm{f}x_\mathrm{b})\left.\frac{\partial^4\Phi}{\partial x^4}\right|_{ij} - \frac{1}{60}(x_\mathrm{f}-x_\mathrm{b})(x_\mathrm{f}^2+x_\mathrm{b}^2)\left.\frac{\partial^5\Phi}{\partial x^5}\right|_{ij} + O\left(\frac{x_\mathrm{f}^5+x_\mathrm{b}^5}{x_\mathrm{f}+x_\mathrm{b}}\right) \tag{4}$$

In the x-direction, the first- and second-order central difference operators are defined by

$$\delta_x\Phi_{ij} = \frac{\Phi_{i+1,j}-\Phi_{i-1,j}}{x_\mathrm{f}+x_\mathrm{b}} \quad \text{and} \quad \delta_x^2\Phi_{ij} = \frac{2}{(x_\mathrm{f}+x_\mathrm{b})}\left[\frac{\Phi_{i+1,j}}{x_\mathrm{f}}+\frac{\Phi_{i-1,j}}{x_\mathrm{b}}-\left(\frac{1}{x_\mathrm{f}}+\frac{1}{x_\mathrm{b}}\right)\Phi_{i,j}\right]$$

With these notations, (4) becomes

$$\left.\frac{\partial^2\Phi}{\partial x^2}\right|_{ij} = \delta_x^2\Phi_{ij} - \frac{1}{3}(x_\mathrm{f}-x_\mathrm{b})\left.\frac{\partial^3\Phi}{\partial x^3}\right|_{ij} - \frac{1}{12}(x_\mathrm{f}^2+x_\mathrm{b}^2-x_\mathrm{f}x_\mathrm{b})\left.\frac{\partial^4\Phi}{\partial x^4}\right|_{ij}$$
$$-\frac{1}{60}(x_\mathrm{f}-x_\mathrm{b})(x_\mathrm{f}^2+x_\mathrm{b}^2)\left.\frac{\partial^5\Phi}{\partial x^5}\right|_{ij} + O\left(\frac{x_\mathrm{f}^5+x_\mathrm{b}^5}{x_\mathrm{f}+x_\mathrm{b}}\right) \tag{5}$$

From Equations (3) and (5), the first derivative may be approximated as

$$\left.\frac{\partial\Phi}{\partial x}\right|_{ij} = \delta_x\Phi_{ij} - \frac{1}{2}(x_\mathrm{f}-x_\mathrm{b})\delta_x^2\Phi_{ij} - \frac{x_\mathrm{f}x_\mathrm{b}}{6}\left.\frac{\partial^3\Phi}{\partial x^3}\right|_{ij}$$
$$-\frac{1}{24}x_\mathrm{f}x_\mathrm{b}(x_\mathrm{f}-x_\mathrm{b})\left.\frac{\partial^4\Phi}{\partial x^4}\right|_{ij} + O\left(\frac{x_\mathrm{f}^5+x_\mathrm{b}^5}{x_\mathrm{f}+x_\mathrm{b}}\right) \tag{6}$$

Similar expressions can be derived for the y-derivatives.

Now, we proceed to derive the HOC scheme for the 2D convection–diffusion equation on non-uniform grids. The steady-state 2D convection–diffusion equation in a transport variable ϕ can be written as

$$-\nabla^2\phi + c\frac{\partial\phi}{\partial x} + d\frac{\partial\phi}{\partial y} = f(x,y) \tag{7}$$

where $\nabla^2 \equiv \partial^2/\partial x^2 + \partial^2/\partial y^2$, c and d are variable or constant convective coefficients in the x- and y-directions respectively and f is a forcing function. In view of Equations (5) and (6), the last equation may be approximated at the point (i, j) as

$$[-\delta_x^2 - \delta_y^2 + c\{\delta_x - 0.5(x_\mathrm{f} - x_\mathrm{b})\delta_x^2\} + d\{\delta_y - 0.5(y_\mathrm{f} - y_\mathrm{b})\delta_y^2\}]\phi_{ij} + \tau_{ij} = f_{ij} \tag{8}$$

where τ_{ij} is the truncation error given by

$$\tau_{ij} = H_1 \frac{\partial^3 \phi}{\partial x^3} + K_1 \frac{\partial^3 \phi}{\partial y^3} + H_2 \frac{\partial^4 \phi}{\partial x^4} + K_2 \frac{\partial^4 \phi}{\partial y^4} + (x_\mathrm{f} - x_\mathrm{b})(x_\mathrm{f}^2 + x_\mathrm{b}^2)\phi_1$$

$$+ (y_\mathrm{f} - y_\mathrm{b})(y_\mathrm{f}^2 + y_\mathrm{b}^2)\phi_2 + O\left(\frac{x_\mathrm{f}^5 + x_\mathrm{b}^5}{x_\mathrm{f} + x_\mathrm{b}}\right) \tag{9}$$

with ϕ_1, ϕ_2 being the leading truncation error terms and

$$H_1 = \tfrac{1}{6}\{2(x_\mathrm{f} - x_\mathrm{b}) - cx_\mathrm{f}x_\mathrm{b}\}, \quad H_2 = \tfrac{1}{24}\{2(x_\mathrm{f}^2 + x_\mathrm{b}^2 - x_\mathrm{f}x_\mathrm{b}) - cx_\mathrm{f}x_\mathrm{b}(x_\mathrm{f} - x_\mathrm{b})\}$$

and

$$K_1 = \tfrac{1}{6}\{2(y_\mathrm{f} - y_\mathrm{b}) - dy_\mathrm{f}y_\mathrm{b}\}, \quad K_2 = \tfrac{1}{24}\{2(y_\mathrm{f}^2 + y_\mathrm{b}^2 - y_\mathrm{f}y_\mathrm{b}) - dy_\mathrm{f}y_\mathrm{b}(y_\mathrm{f} - y_\mathrm{b})\}$$

2.1. Constant convective coefficients

If the convective coefficients c and d are constants, using the original Equation (7) to substitute for the third- and fourth-order derivatives, (9) can be written as

$$\tau_{ij} = (H_1 + H_2 c)c \frac{\partial^2 \phi}{\partial x^2} + (K_1 + K_2 d)d \frac{\partial^2 \phi}{\partial y^2} + \{(H_1 + H_2 c)d + (K_1 + K_2 d)c\} \frac{\partial^2 \phi}{\partial x \partial y}$$

$$- (H_1 + H_2 c - K_2 c) \frac{\partial^3 \phi}{\partial x \partial y^2} - (K_1 + K_2 d - H_2 d) \frac{\partial^3 \phi}{\partial x^2 \partial y} - (H_2 + K_2) \frac{\partial^4 \phi}{\partial x^2 \partial y^2}$$

$$- \left\{(H_1 + H_2 c) \frac{\partial}{\partial x} + (K_1 + K_2 d) \frac{\partial}{\partial y} + H_2 \frac{\partial^2}{\partial x^2} + K_2 \frac{\partial^2}{\partial y^2}\right\} f$$

$$+ (x_\mathrm{f} - x_\mathrm{b})(x_\mathrm{f}^2 + x_\mathrm{b}^2)\phi_1 + (y_\mathrm{f} - y_\mathrm{b})(y_\mathrm{f}^2 + y_\mathrm{b}^2)\phi_2 + O\left(\frac{x_\mathrm{f}^5 + x_\mathrm{b}^5}{x_\mathrm{f} + x_\mathrm{b}}\right) \tag{10}$$

From Equations (8) and (10), the HOC scheme on non-uniform grids for Equation (7) can now be written as

$$[-A_{ij}\delta_x^2 - B_{ij}\delta_y^2 + c\delta_x + d\delta_y + G_{ij}\delta_x\delta_y - H_{ij}\delta_x\delta_y^2 - K_{ij}\delta_x^2\delta_y - L_{ij}\delta_x^2\delta_y^2]\phi_{ij} = F_{ij} \tag{11}$$

where the coefficients $A_{ij}, B_{ij}, G_{ij}, H_{ij}, K_{ij}$ and L_{ij} are as follows:

$$A_{ij} = 1 + 0.5(x_\mathrm{f} - x_\mathrm{b})c - (H_1 + H_2 c)c \tag{12}$$

$$B_{ij} = 1 + 0.5(y_\mathrm{f} - y_\mathrm{b})d - (K_1 + K_2 d)d \tag{13}$$

$$G_{ij} = (H_1 + H_2 c)d + (K_1 + K_2 d)c \tag{14}$$

$$H_{ij} = H_1 + H_2 c - K_2 c \tag{15}$$

$$K_{ij} = K_1 + K_2 d - H_2 d \tag{16}$$

$$L_{ij} = H_2 + K_2 \tag{17}$$

and

$$F_{ij} = [1 + (H_1 + H_2 c)\delta_x + (K_1 + K_2 d)\delta_y + \{H_2 - 0.5(x_\mathrm{f} - x_\mathrm{b})(H_1 + H_2 c)\}\delta_x^2 + \{K_2 - 0.5(y_\mathrm{f} - y_\mathrm{b})(K_1 + K_2 d)\}\delta_y^2] f_{ij} \tag{18}$$

2.2. Variable convective coefficients

For variable convective coefficients the formulations are more complicated with the derivatives of c and d also coming into the picture. Using (7), as before, to substitute for the derivatives, (9) can be written as

$$\begin{aligned}
\tau_{ij} = {} & \left(H_1 c + H_2 c^2 + 2H_2 \frac{\partial c}{\partial x}\right)\frac{\partial^2 \phi}{\partial x^2} + \left(K_1 d + K_2 d^2 + 2K_2 \frac{\partial d}{\partial y}\right)\frac{\partial^2 \phi}{\partial y^2} \\
& + \left\{(H_1 + H_2 c)\frac{\partial c}{\partial x} + (K_1 + K_2 d)\frac{\partial c}{\partial y} + H_2 \frac{\partial^2 c}{\partial x^2} + K_2 \frac{\partial^2 c}{\partial y^2}\right\}\frac{\partial \phi}{\partial x} \\
& + \left\{(H_1 + H_2 c)\frac{\partial d}{\partial x} + (K_1 + K_2 d)\frac{\partial d}{\partial y} + H_2 \frac{\partial^2 d}{\partial x^2} + K_2 \frac{\partial^2 d}{\partial y^2}\right\}\frac{\partial \phi}{\partial y} \\
& + \left\{(H_1 + H_2 c)d + (K_1 + K_2 d)c + 2H_2 \frac{\partial d}{\partial x} + 2K_2 \frac{\partial c}{\partial y}\right\}\frac{\partial^2 \phi}{\partial x \partial y} \\
& - \{H_1 + H_2 c - K_2 c\}\frac{\partial^3 \phi}{\partial x \partial y^2} - \{K_1 + K_2 d - H_2 d\}\frac{\partial^3 \phi}{\partial x^2 \partial y} \\
& - (H_2 + K_2)\frac{\partial^4 \phi}{\partial x^2 \partial y^2} - \left\{(H_1 + H_2 c)\frac{\partial}{\partial x} + (K_1 + K_2 d)\frac{\partial}{\partial y} + H_2 \frac{\partial^2}{\partial x^2} + K_2 \frac{\partial^2}{\partial y^2}\right\} f \\
& + (x_\mathrm{f} - x_\mathrm{b})(x_\mathrm{f}^2 + x_\mathrm{b}^2)\phi_1 + (y_\mathrm{f} - y_\mathrm{b})(y_\mathrm{f}^2 + y_\mathrm{b}^2)\phi_2 + O\left(\frac{x_\mathrm{f}^5 + x_\mathrm{b}^5}{x_\mathrm{f} + x_\mathrm{b}}\right)
\end{aligned} \tag{19}$$

From Equations (8) and (19), we have the following HOC scheme on non-uniform grids for Equation (7):

$$[-A_{ij}\delta_x^2 - B_{ij}\delta_y^2 + C_{ij}\delta_x + D_{ij}\delta_y + G_{ij}\delta_x\delta_y - H_{ij}\delta_x\delta_y^2 - K_{ij}\delta_x^2\delta_y - L_{ij}\delta_x^2\delta_y^2]\phi_{ij} = F_{ij} \tag{20}$$

where the coefficients C_{ij}, D_{ij}, A_{ij}, B_{ij} and G_{ij} are given by

$$C_{ij} = [1 + (H_1 + H_2 c)\delta_x + (K_1 + K_2 d)\delta_y + \{H_2 - 0.5(x_\mathrm{f} - x_\mathrm{b})(H_1 + H_2 c)\}\delta_x^2 + \{K_2 - 0.5(y_\mathrm{f} - y_\mathrm{b})(K_1 + K_2 d)\}\delta_y^2]c \tag{21}$$

$$D_{ij} = [1 + (H_1 + H_2 c)\delta_x + (K_1 + K_2 d)\delta_y + \{H_2 - 0.5(x_f - x_b)(H_1 + H_2 c)\}\delta_x^2 + \{K_2 - 0.5(y_f - y_b)(K_1 + K_2 d)\}\delta_y^2]d \tag{22}$$

$$A_{ij} = 1 - [(H_1 + H_2 c)c + 2H_2\{\delta_x c - 0.5(x_f - x_b)\delta_x^2 c\}] + 0.5(x_f - x_b)C_{ij} \tag{23}$$

$$B_{ij} = 1 - [(K_1 + K_2 d)d + 2K_2\{\delta_y d - 0.5(y_f - y_b)\delta_y^2 d\}] + 0.5(y_f - y_b)D_{ij} \tag{24}$$

and

$$G_{ij} = (H_1 + H_2 c)d + (K_1 + K_2 d)c + 2H_2\delta_x d + 2K_2\delta_y c - \{H_2(x_f - x_b)\delta_x^2 d + K_2(y_f - y_b)\delta_y^2 c\} \tag{25}$$

The expressions for τ_{ij} in Equations (10) and (19) clearly indicate that the local order of accuracy of the scheme is four or three depending upon the grid spacing. The order of the truncation error is four on uniform grids (when $x_f = x_b$ and $y_f = y_b$) and at least three when the grid spacing is non-uniform (when $x_f \neq x_b$ or $y_f \neq y_b$).

The details of the finite difference operators appearing in Equations (11) and (20) are given in the Appendix. The discretized form of Equations (11) and (20) can now be written as

$$\sum_{k_1=-1}^{1}\sum_{k_2=-1}^{1}\eta_{i+k_1,j+k_2}\phi_{i+k_1,j+k_2} = \sum_{k_1=-1}^{1}\sum_{k_2=-1}^{1}\xi_{i+k_1,j+k_2}f_{i+k_1,j+k_2} \tag{26}$$

where η, ξ's are functions of the convective coefficients c and d, their derivatives and the step lengths x_f, x_b, y_f and y_b. In matrix form, the system of algebraic equations given by (26) can now be written as

$$A\mathbf{\Phi} = \mathbf{F} \tag{27}$$

where the coefficient matrix A is an asymmetric sparse matrix with each row containing at most nine non-zero entries. For a grid of size $m \times n$, A is of size $mn \times mn$, and $\mathbf{\Phi}$ and $\mathbf{F}$ are mn-component vectors. Partitioning A, $\mathbf{\Phi}$ and $\mathbf{F}$ into sub-matrices corresponding to the interior and the boundaries, Equation (27) can be written as

$$\begin{pmatrix} A_L & O & O & O & O \\ O & A_B & O & O & O \\ O & O & A_D & O & O \\ O & O & O & A_T & O \\ O & O & O & O & A_R \end{pmatrix} \begin{pmatrix} \mathbf{\Phi}_L \\ \mathbf{\Phi}_B \\ \mathbf{\Phi}_D \\ \mathbf{\Phi}_T \\ \mathbf{\Phi}_R \end{pmatrix} = \begin{pmatrix} \mathbf{F}_L \\ \mathbf{F}_B \\ \mathbf{F}_D \\ \mathbf{F}_T \\ \mathbf{F}_R \end{pmatrix}$$

where suffixes L, R, B and T stand, respectively, for the left, right, bottom and top boundaries of the domain and D represents the interior. Here, O's are rectangular null matrices of orders ranging from $m \times (n-2)$ to $m \times (m-2)(n-2)$. The block square matrices A_B and A_T are of order m, A_L and A_R are of order $(n-2)$, and A_D is of order $(m-2)(n-2)$. If Dirichlet boundary conditions are prescribed, the sub-matrices representing the boundary conditions are identity matrices. For Neumann boundary conditions, they will be sparse matrices with the number of non-zero entries in a particular row depending upon the order of the boundary

difference scheme. The details of the elements of the column vectors on the left-hand side are as follows:

$$[\mathbf{\Phi}_{\mathrm{L}}]=[\phi_{1,2},\ldots,\phi_{1,n-1}]^{\tau},\quad [\mathbf{\Phi}_{\mathrm{B}}]=[\phi_{1,1},\ldots,\phi_{m,1}]^{\tau}$$

$$[\mathbf{\Phi}_{\mathrm{T}}]=[\phi_{1,n},\ldots,\phi_{m,n}]^{\tau},\qquad [\mathbf{\Phi}_{\mathrm{R}}]=[\phi_{m,2},\ldots,\phi_{m,n-1}]^{\tau}$$

and

$$[\mathbf{\Phi}_{\mathrm{D}}]=[\phi_{2,2},\ldots,\phi_{m-1,2},\phi_{2,3},\ldots,\phi_{m-1,3},\ldots,\phi_{2,n-1},\ldots,\phi_{m-1,n-1}]^{\tau}$$

Similarly, the vectors $[\mathbf{F}_{\mathrm{L}}]_{(n-2)\times 1}$, $[\mathbf{F}_{\mathrm{R}}]_{(n-2)\times 1}$, $[\mathbf{F}_{\mathrm{B}}]_{m\times 1}$ and $[\mathbf{F}_{\mathrm{T}}]_{m\times 1}$ correspond respectively to the left, right, bottom and top boundary conditions, and the entries of $[\mathbf{F}_{\mathrm{D}}]_{(m-2)(n-2)\times 1}$ are given by the right-hand side of Equation (26).

The next step is to solve Equation (27) with iterative methods. As the coefficient matrix A is generally not diagonally dominant, conventional iterative methods such as Gauss–Seidel cannot be used. On uniform grids, some of the associated matrices are symmetric and positive definite, which allows algorithms like conjugate gradient (CG) [16] to be used. As non-uniform grid invariably leads to unsymmetric matrices, in order to solve these systems, the hybrid biconjugate gradient stabilized method (BiCGStab(2)) [16] is used without preconditioning. For a problem having Dirichlet boundary conditions, A will have at most $2[m+n-2]+9\times(m-2)(n-2)$ non-zero entries. Therefore, for such iterative methods, the computation of the matrix-vector product $A\mathbf{\Phi}$ involves $2[m+n-2]+81\times(m-2)(n-2)$ arithmetic operations only.

It may be noted that for the coupled non-linear PDEs (such as the ψ-ω form of the N–S equations), an iterative solution procedure must be adopted. These iterations may be termed as outer iterations. We use a decoupled algorithm where vorticity and stream functions are solved iteratively and sequentially through hybrid BiCGStab(2) and lagging the appropriate terms. The latter iterations may be termed inner iterations which must be carried out at every outer iteration with updated data.

3. NUMERICAL TEST CASES

The proposed scheme has been applied to two linear and one non-linear test cases. The non-linear case deals with fluid flows governed by the 2D steady-state incompressible N–S equations. Care has been taken to choose such problems as will permit the use of non-uniform grids at certain portions of the solution domain for better scale resolution and grid economy. Both Dirichlet and Neumann boundary conditions have been used wherever necessary.

3.1. Problem 1: Gartland model problem

We take the problem proposed by Gartland [17], where in Equation (7),

$$c=Re,\quad d=0,\quad f=0\quad \forall\ 0\leqslant x,y\leqslant 1$$

with boundary conditions

$$\phi(x,0)=\phi(x,1)=0\quad 0\leqslant y\leqslant 1$$

$$\phi(0,y)=\sin\pi y,\quad \phi(1,y)=2\sin\pi y\quad 0\leqslant x\leqslant 1$$

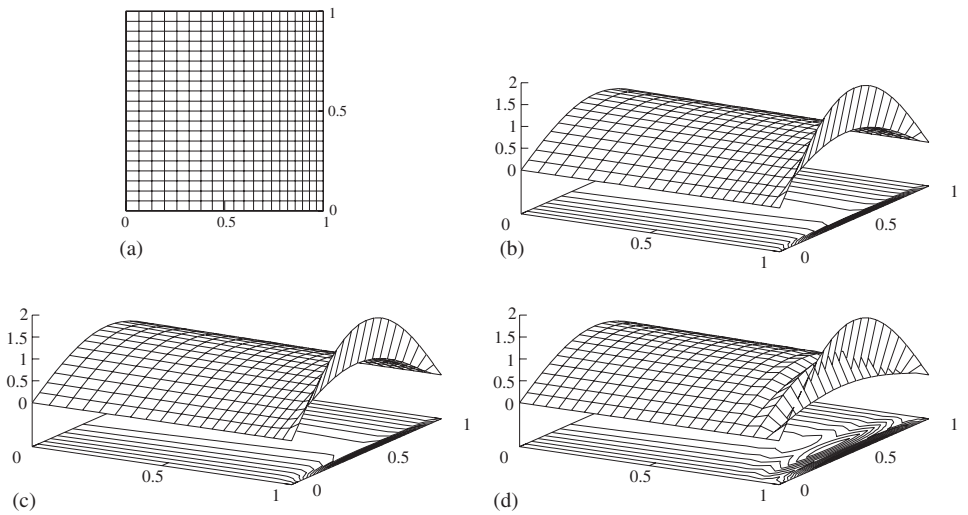

Figure 2. For problem 1, at $Re = 100$: (a) the grid used (21×21), the surface and contour plots of (b) the exact and numerical solutions with (c) the present ($\lambda = 0.5$) and (d) the CD scheme.

The exact solution is given by

$$\phi(x, y) = e^{Rex/2} \sin \pi y \, \frac{2e^{-Re/2} \sinh \sigma x + \sinh \sigma(1 - x)}{\sinh \sigma}, \quad \sigma^2 = \pi^2 + \frac{Re^2}{4} \tag{28}$$

The solution has a boundary layer attached to the line $x = 1$ and therefore, a uniform grid along the y-direction, and a non-uniform grid along the x-direction with clustering near $x = 1$ has been used with the following stretching function [8]

$$x_i = \frac{i}{i_{\max}} + \frac{\lambda}{\pi} \sin\left(\frac{\pi i}{i_{\max}}\right)$$

where λ is a stretching parameter controlling the density of grid points in the x-direction. It may be noted that higher the value of λ, greater the clustering near the boundary. The grid is shown in Figure 2(a). Figures 2(b), (c) and (d), respectively, show the surface and contour plots of the exact, the numerical solution with the present scheme ($\lambda = 0.5$) and the numerical solution with the central difference (CD) scheme on a 21×21 grid for $Re = 100$. While the numerical solution with the present scheme shows no discernable differences with the exact solution, the CD solution shows a clear oscillation in the region of the boundary layer. This is attributed to the violation of the so-called cell-Péclect condition

$$Re_{\Delta x} = Re \Delta x < 2 \quad \text{or} \quad \Delta x < \frac{2}{Re}$$

On the other hand the maximum and the minimum values of Δx with our scheme are 0.064 and 0.045, which being greater than the limit 0.02, clearly violates the above condition. In spite of this violation, no oscillation is seen in the results indicating that the present scheme has the

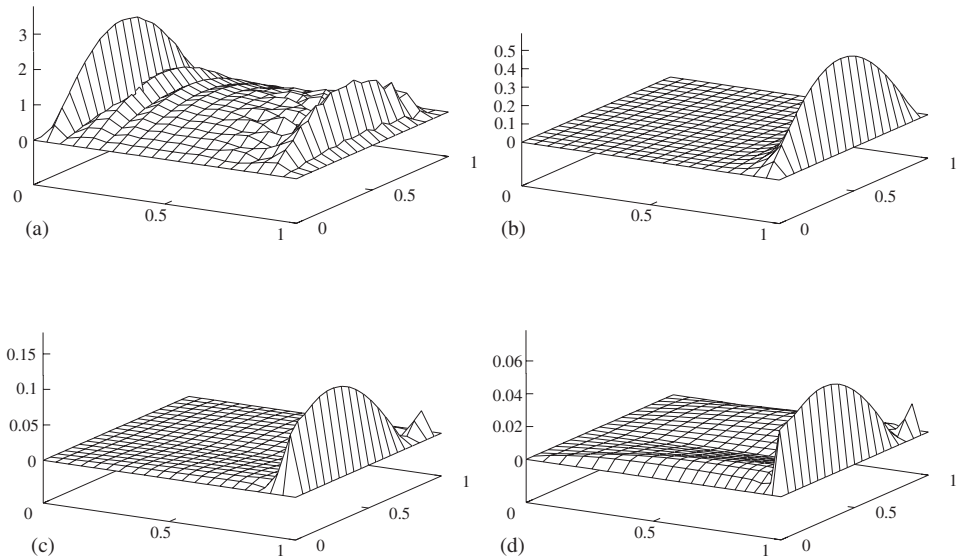

Figure 3. Surface plots of the absolute errors for problem 1 ($Re = 100, 21 \times 21$ grid): (a) upwind; (b) central difference; (c) uniform HOC; and (d) present ($\lambda = 0.5$) scheme.

oscillation suppressing property.[††] Also the surface plots of the absolute errors (Figure 3) for the upwind, CD, HOC uniform and the present scheme for the same configuration confirms that, amongst them, the present scheme yields the best result. Table I compares the absolute errors (abs(er)) at specific points and the maximum errors (max(er)) on different grid sizes for different stretching parameters. Because of the clustering in the boundary layer region, the maximum errors for the present scheme for all λ's are lower than the maximum error on uniform grids and it decreases with increasing λ values. It is seen from Table I that with grid refinement, the point-wise error decays with $O(h^M)$, where $3 \leqslant M \leqslant 4$ as expected. Here M is calculated as

$$M = \frac{\log(e_1/e_2)}{\log(N_2/N_1)}$$

where e_1, e_2 are the absolute errors estimated at a particular point for two different grids with $N_1 + 1$ and $N_2 + 1$ points in the x-direction. The maximum errors for different grids occur at different points for the same range of parameters and are not directly comparable. In any case the maximum error from the data exhibits a better than $O(h^2)$ rate of convergence.

[††]A rigorous adjacent slope ratio analysis reveals that the scheme for the one-dimensional case (to be discussed in a separate paper) is non-oscillatory if the ratio of the forward and backward step lengths

$$x_f : x_b \in \left(2 - \frac{2}{\sqrt{3}}, \frac{5-\sqrt{3}}{2}\right) \cup \left(\frac{1}{2} - \frac{1}{2\sqrt{3}}, \frac{3-\sqrt{5}}{2}\right) \cup \left(\frac{3+\sqrt{5}}{2}, \frac{5+\sqrt{3}}{2}\right)$$

Table I. Comparison of errors on uniform and non-uniform grids for Problem 1 for $Re = 100$.

	Uniform ($\lambda = 0.0$)			
Grid	abs(er) at $(0.5, 0.5)$	abs(er) at $(0.75, 0.5)$	abs(er) at $(0.96875, 0.5)$	max(er)
33×33	1.18×10^{-4}	1.70×10^{-4}	3.30×10^{-2}	4.06×10^{-2}
65×65	7.44×10^{-6}	1.07×10^{-5}	1.41×10^{-3}	6.81×10^{-3}
129×129	4.65×10^{-7}	6.71×10^{-7}	7.94×10^{-5}	1.30×10^{-3}
Grid		Non-uniform ($\lambda = 0.5$)		
	abs(er) at $(0.5002, 0.5)$	abs(er) at $(0.7428, 0.5)$	abs(er) at $(0.9783, 0.5)$	max(er)
33×33	2.69×10^{-4}	3.06×10^{-4}	1.03×10^{-2}	1.37×10^{-2}
65×65	1.73×10^{-5}	1.98×10^{-5}	5.41×10^{-4}	2.69×10^{-3}
129×129	1.09×10^{-6}	1.26×10^{-6}	3.24×10^{-5}	5.54×10^{-4}
Grid		Non-uniform ($\lambda = 0.7$)		
	abs(er) at $(0.5019, 0.5)$	abs(er) at $(0.7519, 0.5)$	abs(er) at $(0.9822, 0.5)$	max(er)
33×33	3.75×10^{-4}	4.16×10^{-4}	5.18×10^{-3}	7.71×10^{-3}
65×65	2.44×10^{-5}	2.72×10^{-5}	2.91×10^{-4}	1.60×10^{-3}
129×129	1.54×10^{-6}	1.73×10^{-6}	1.76×10^{-5}	3.51×10^{-4}
Grid		Non-uniform ($\lambda = 0.9$)		
	abs(er) at $(0.4995, 0.5)$	abs(er) at $(0.7628, 0.5)$	abs(er) at $(0.9861, 0.5)$	max(er)
33×33	5.12×10^{-4}	5.65×10^{-4}	2.05×10^{-3}	4.95×10^{-3}
65×65	3.37×10^{-5}	3.74×10^{-5}	1.24×10^{-4}	1.24×10^{-3}
129×129	2.13×10^{-6}	2.38×10^{-6}	7.81×10^{-6}	3.12×10^{-4}

3.2. Problem 2: 2D linear convection–diffusion

We take the problem where in Equation (7),

$$c = Re\cos\theta, \quad d = Re\sin\theta \quad \text{and} \quad f = 0 \qquad 0 \leqslant x \leqslant 1, \quad 0 \leqslant y \leqslant 1$$

with boundary conditions

$$\phi(x, 0) = \phi(x, 1) = 0 \quad 0 \leqslant x \leqslant 1$$

$$\phi(0, y) = 4y(1 - y) \quad \phi(1, y) = 0, \quad 0 \leqslant y \leqslant 1$$

This problem has the exact solution

$$\phi(x, y) = \exp\left(-\frac{Re}{2}(x\cos\theta + y\sin\theta)\right)\sum_{n=1}^{\infty}\{B_n \sinh[\sigma_n(1 - x)]\sin(n\pi y)\} \tag{29}$$

where

$$\sigma_n^2 = n^2\pi^2 + \frac{Re^2}{4}$$

and

$$B_n = \frac{8}{\sinh\sigma_n}\int_0^1 y(1 - y)\exp\left(\frac{-Re}{2}\, y\sin\theta\right)\sin(n\pi y)\,\mathrm{d}y$$

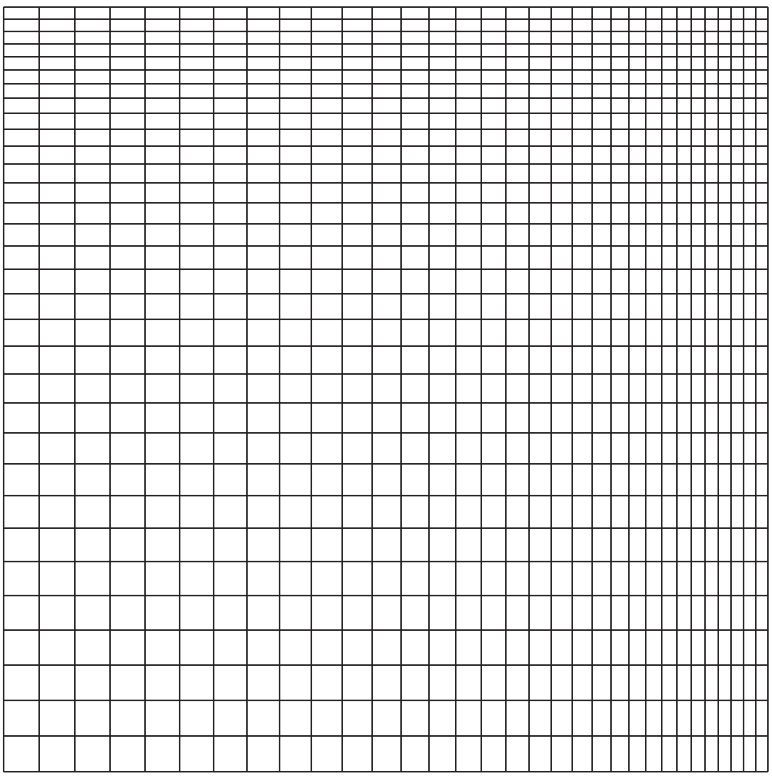

Figure 4. Grid used (32×32) for Problem 2.

It deals with the convection of ϕ (temperature or concentration) in a fluid moving with a uniform velocity at an angle θ to the x-axis. It has earlier been solved numerically by Gupta *et al.* [18] and Mackinnon and Johnson [6]. For non-zero values of θ, the solution has boundary layers near $x=1$ and $y=1$. For $\theta=0$, convection is along x-axis only resulting in the development of boundary layers near $x=1$. The present computation uses the following stretching function (see Reference [14]) in both x- and y-directions to generate clustered grids with refinement near $x=1$ and $y=1$ (Figure 4)

$$x_i = \frac{i}{i_{\max}} + \frac{\lambda}{\pi} \sin\left(\frac{\pi i}{i_{\max}}\right), \quad 0 < \lambda \leqslant 1$$

where λ is a stretching parameter controlling the density of grid points in the x-direction. It may be noted that higher the value of λ, greater the clustering near the boundary. The method captures the boundary layers very well as can be seen from Figure 5 where the computed contours of ϕ has been plotted for two convection angles $\pi/4$ and $\pi/8$. Table II compares the maximum error (max(er)) for $Re=40$ for three convection angles, viz. $\pi/4$, $\pi/8$ and 0 with those obtained from the Upwind Difference Scheme (UDS), the Central Difference Scheme (CDS), and the higher order schemes of Spotz and Carey [5] and Gupta *et al.* [18]

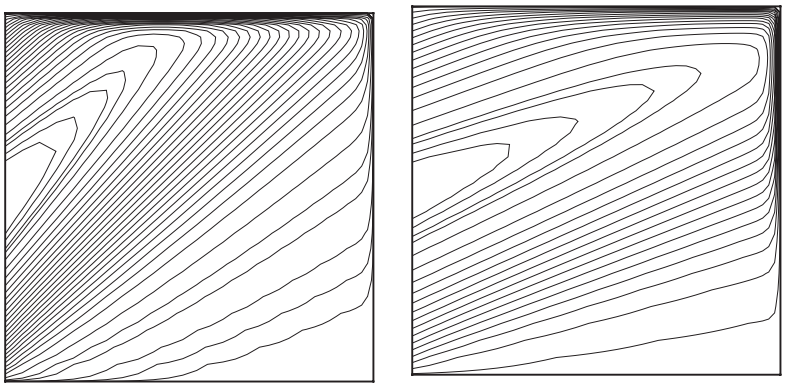

(a) (b)

Figure 5. Contour plots of ϕ in Problem 2 for $Re = 80$: (a) $\theta = \pi/4$; and (b) $\theta = \pi/8$.

Table II. Comparison of the maximum errors of different schemes for 2D linear convection–diffusion.

θ	Grid size	UDS $O(h)$	CDS $O(h^2)$	Gupta *et al.* $O(h^4)$	Spotz and Carey $O(h^4)$	Present ($\lambda = 0.8$) $O(h^\alpha)$ ($\alpha = 3$ or 4)
0	16×16	0.1604	0.1532	0.01323	0.04050	0.01314
	32×32	0.1256	0.0445	0.00112	0.00856	0.00302
$\frac{\pi}{8}$	16×16	0.2268	0.1286	0.01019	0.01769	0.03002
	32×32	0.1394	0.0348	0.00081	0.00492	0.00759
$\frac{\pi}{4}$	16×16	0.2035	0.0803	0.00598	0.00598	0.00487
	32×32	0.1218	0.0195	0.00041	0.00041	0.00045

for different grid sizes. When judged against the orders of accuracy of the other schemes, the errors of the present computations are within the expected limits.

3.3. Problem 3: Lid-driven cavity flow

The solution procedure is now extended to the 2D laminar lid-driven square cavity problem which has been used extensively to study the strength and accuracy of numerical methods for incompressible flow problems. This flow is governed by the 2D incompressible N–S equations. The stream function-vorticity (ψ–ω) form of these equations has been used in the present computations. The geometry and the boundary conditions have been shown in Figure 6 where the top wall is moving from left to right and the remaining three walls are stationary. The flow is driven by the moving wall and the resultant flow patterns depend on *Re*. Because of the presence of large gradients near the walls, grid has been clustered there using the stretching function

$$x_i = \frac{i}{i_{\max}} - \frac{\lambda}{2\pi} \sin\left(\frac{2\pi i}{i_{\max}}\right), \quad 0 < \lambda \leqslant 1$$

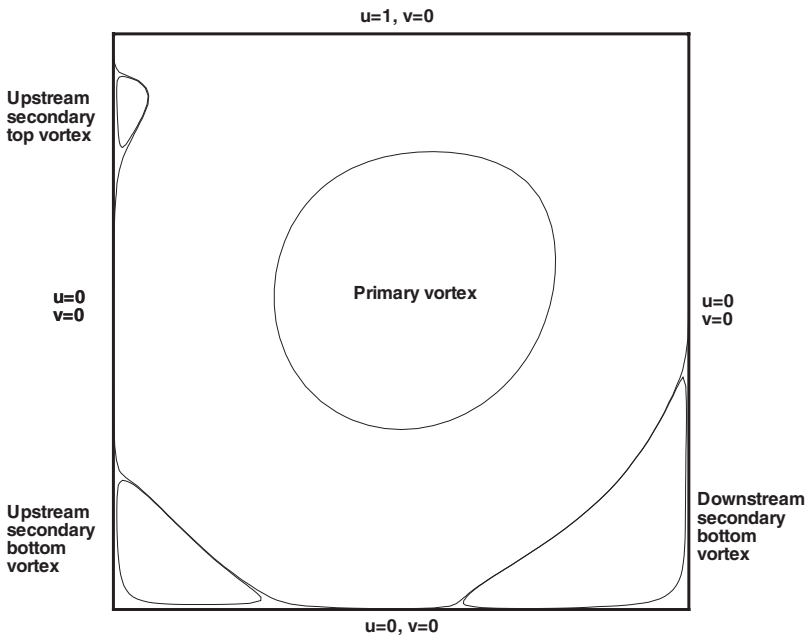

Figure 6. The lid-driven cavity flow configuration with boundary conditions.

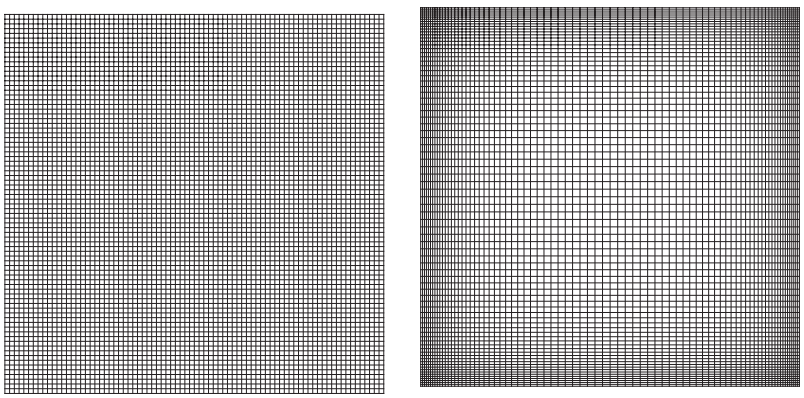

Figure 7. 81×81 grids for square cavity: (a) uniform; and (b) clustered with $\lambda = 0.6$.

which we obtain by combining the functions used by Spotz and Carey [14] and Janssen and Henkes [19]. Here, the parameter λ determines the degree of clustering near the boundaries with centrosymmetric stretching. The effect of λ on grids can be seen from Figures 7(a) and (b) where a uniform and a clustered 81×81 grid have been shown. Numerical results are presented for Re's ranging from 100 to 7500 with grid sizes varying from 11×11 to 121×121. As the boundary layer thickness is of the order of $Re^{-0.5}$, grid size and λ have been chosen in

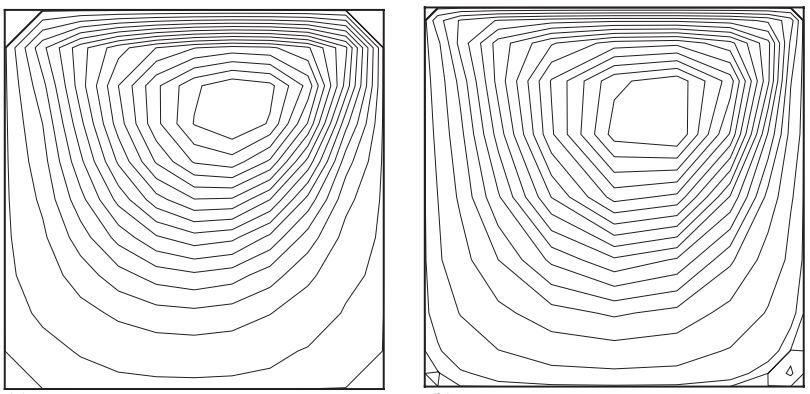

Figure 8. Streamlines for the lid-driven cavity flow on 11×11 grid for $Re = 100$: (a) uniform HOC; and (b) present scheme ($\lambda = 0.7$).

such a way that there are several points within the boundary layer. For example, the minimum internodal distance near the wall is 0.0345 for $Re = 100$ ($11 \times 11, \lambda = 0.7$) and 1.37×10^{-4} for $Re = 3200$ ($81 \times 81, \lambda = 0.99$). The Neumann boundary conditions for vorticity are obtained through a third-order compact formula [5] as a fourth-order compact boundary scheme is found to be oscillatory at the moving wall. For $Re = 100$ the streamline contours obtained by HOC schemes on 11×11 uniform and non-uniform grids are shown in Figures 8(a) and (b). It is clear from the figures that the fourth-order accurate scheme on uniform grids captures none of the corner vortices whereas the present scheme with accuracy lower than fourth does. Interestingly the present scheme with a grid as coarse as 21×21 ($\lambda = 0.6$) captures the flow details quite accurately as can be seen from the comparison with the results of Ghia *et al.* [20] produced with a 129×129 grid (Figure 9). The centerline velocity profiles obtained through the present scheme with those of Ghia *et al.* [20] are presented side by side in Figure 10 for different *Re*'s. Again it is seen that the present scheme computes the flow with a much coarser grid. The significance of grid clustering at high *Re*'s involving multiple scales can be seen from Figure 11 where for $Re = 3200$, the corner vortex features on 81×81 grids are shown for $\lambda = 0.6$ and 0.99. With $\lambda = 0.6$ (Figure 11(a)), corner vortices only up to the tertiary level have been resolved whereas with $\lambda = 0.99$ two hitherto unreported vortices—the quaternary and post-quaternary-have been captured (Figure 11(b)—walls removed for clarity). Figure 12 shows the streamline contours for $Re = 1000$ and 7500. It is seen that for $Re = 1000$, the present scheme on a 31×31 grid captures even the tertiary vortices (Figure 12(a)—walls removed for clarity) whereas on uniform grid of the same size, iteration stagnates, [5]. Figure 12(b) shows for $Re = 7500$ the general flow features including the top left corner vortex. The following two observations (as also can be seen from Figures 8 and 12), which are in agreement with the earlier investigations [20–23], can be made with increase in *Re*: (i) the primary vortex center shifts from the top right corner towards the geometric center of the cavity and virtually becomes invariant for $Re \geqslant 5000$ (ii) there is an expansion of the recirculation zone for the secondary vortices with a tendency of their centers to shift towards the geometric center. In Table III, the stream function and the vorticity values at the primary vortex centers of the present study have been compared with the calculations of Kim

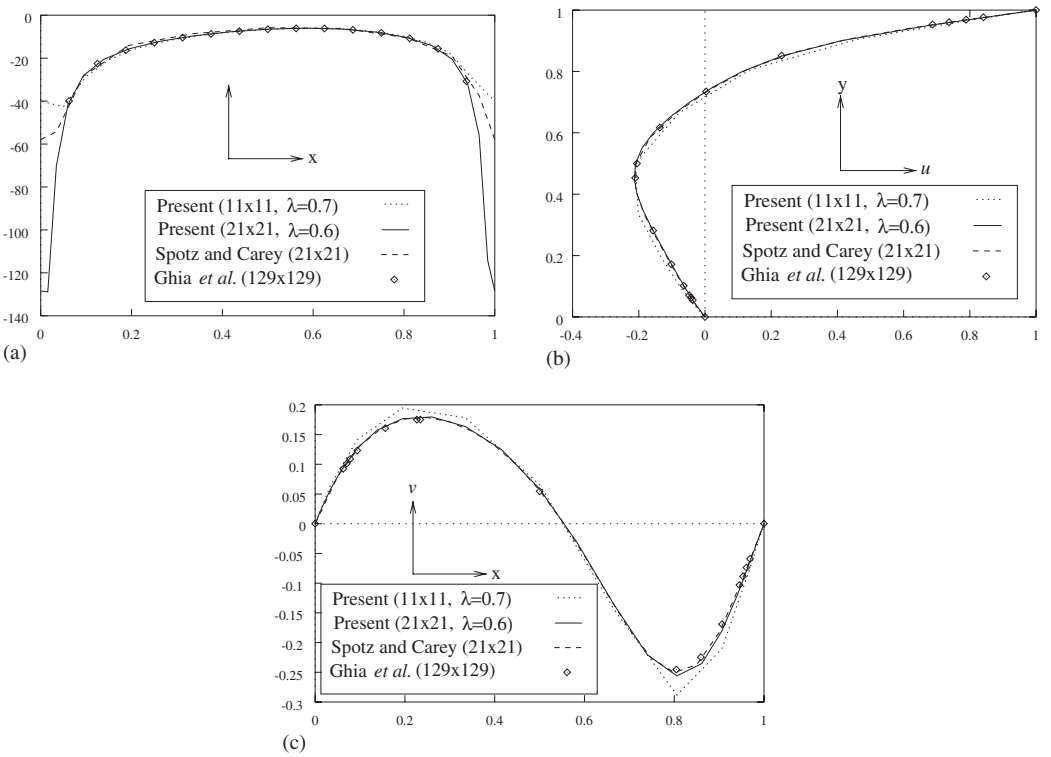

Figure 9. Comparisons of (a) vorticity along the moving wall; (b) horizontal velocity along the vertical centerline; and (c) vertical velocity along the horizontal centerline for $Re = 100$ in the lid-driven cavity flow.

and Moin [21], Ghia *et al.* [20] and Bruneau and Jouron [23] and, agreement has been very close. In Figure 13 the convergence history based on the root mean square error [rms(er)] of ω at $Re = 1000$ for the present scheme for two different grid sizes is shown. This error has been defined as

$$\text{rms(er)} = \left[\frac{1}{i_{\max} \times j_{\max}} \sum (\omega^{(k+1)} - \omega^{(k)})^2 \right]^{1/2}$$

where k and $k+1$ denote two consecutive iteration levels. The CPU times on a Sun enterprise 250 workstation for the two grids are 10.94 and 173.33 s, respectively, when the exit criteria for the fall of residuals of the inner iterations for both ψ and ω are set at 10^{-3}.

4. CONCLUSION

The HOC scheme on non-uniform grids for convection–diffusion has so far been tested only for linear problems with grid transformation. The present work affords an HOC method on non-uniform grids which avoids the complexities associated with transformation. Dispensing

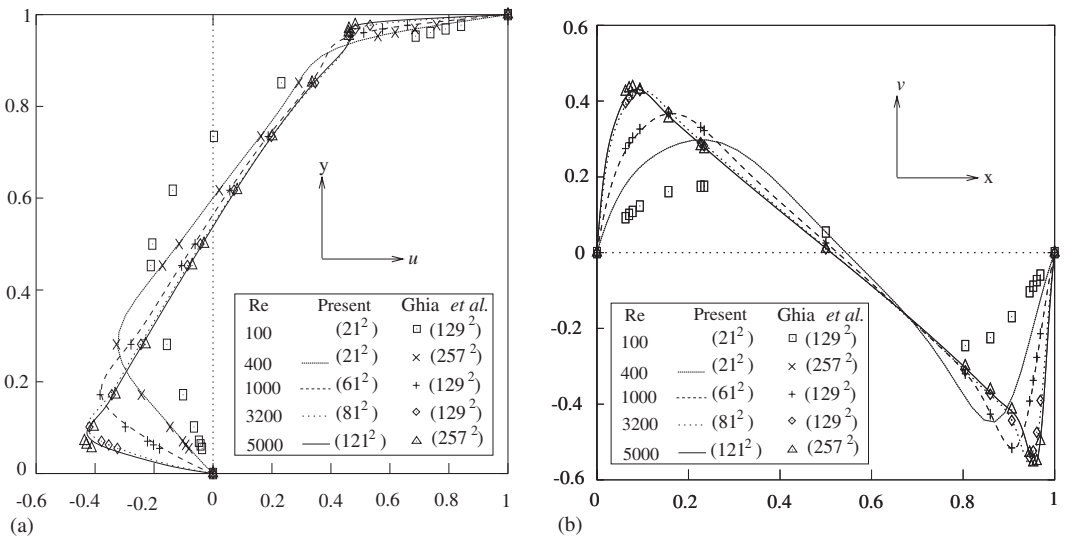

Figure 10. Comparisons of (a) horizontal velocity along the vertical centerline; and (b) vertical velocity along the horizontal centerline for different *Re*'s in the lid-driven cavity flow ($\lambda = 0.6$).

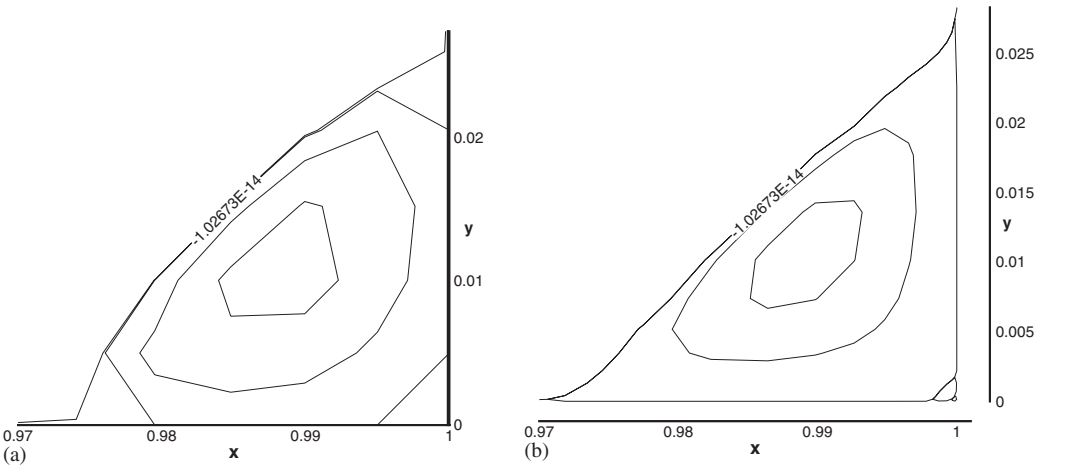

Figure 11. The bottom right vortices for the lid-driven cavity flow at $Re = 3200$ on 81×81 grid: (a) tertiary ($\lambda = 0.6$); and (b) tertiary, quaternary and post-quaternary ($\lambda = 0.99$).

with transformation also reduces computational effort as the method now deals with smaller number of terms at each grid point. Owing to clustering the method is seen to produce accurate solution of complex flows with significantly smaller number of grid points with resultant economy. For instance, a 31×31 grid is found to be good enough to capture the flow details including the tertiary vortices for the lid-driven cavity problem up to $Re = 1000$. The method may therefore, in many respects, be considered superior to similar ones on either

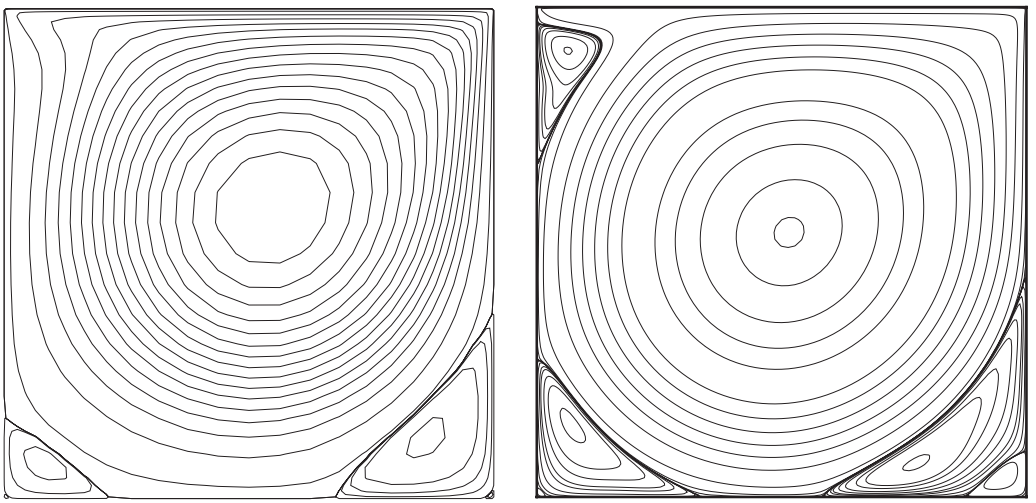

Figure 12. Streamline patterns for the lid-driven cavity flow: (a) $Re = 1000$ $(31 \times 31, \lambda = 0.9)$; and (b) $Re = 7500$ $(121 \times 121, \lambda = 0.6)$.

Table III. Stream function and vorticity at primary vortex center for different *Re*'s.

Re	Kim and Moin	Ghia *et al.*	Bruneau and Jouron	Present ($\lambda = 0.6$)
100	$-0.103(-3.177)$ 65×65	$-0.103(-3.166)$ 129×129	$-0.103(—)$ 128×128	$-0.103(-3.152)$ 41×41
400	$-0.112(-2.260)$ 65×65	$-0.114(-2.295)$ 257×257	— —	$-0.113(-2.260)$ 41×41
1000	$-0.116(-2.026)$ 97×97	$-0.118(-2.050)$ 129×129	$-0.116(—)$ 256×256	$-0.117(-2.057)$ 61×61
3200	$-0.115(-1.901)$ 97×97	$-0.120(-1.989)$ 129×129	— —	$-0.120(-1.962)$ 81×81
5000	$-0.112(-1.812)$ 97×97	$-0.119(-1.860)$ 257×257	$-0.114(—)$ 512×512	$-0.119(-1.926)$ 81×81
7500	— —	$-0.120(-1.880)$ 257×257	$-0.111(—)$ 512×512	$-0.115(-1.874)$ 121×121

uniform grids or non-uniform grids with transformation. Non-uniformity in grid, however, renders the algebraic system for the Poisson equations (for example, those associated with ψ) non-symmetric, necessitating the use of hybrid BiCGStab algorithm instead of CG. We believe that the solution procedure does not lose much competitive edge because of this, as it uses smaller number of grid points which again may become significant at times in terms of saving memory. Since it is possible for the present method to place comparatively larger number of

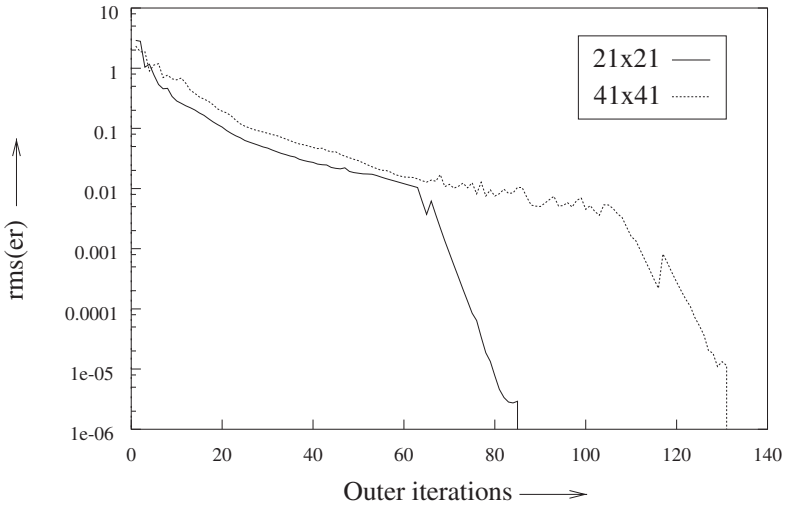

Figure 13. Convergence history based on the root mean square error of ω for $Re = 1000$ ($\lambda = 0.8$) in the lid-driven cavity flow.

grid points in the boundary layer regions, it brings out some unreported features, for example, two new vortices in the much examined lid-driven cavity flow at $Re = 3200$. The solution procedure is very robust and to our knowledge this is the first instance of extension of an HOC algorithm on non-uniform grid to the N–S equations, with or without grid-transformation. Also we believe that the present work, for the first time, effectively extends an HOC algorithm to *Re*'s much beyond 1000 in the lid-driven cavity problem and the method captures very accurate solutions including new flow features. Overall we consider the present method an important addition to the existing solution procedures for incompressible viscous flows.

APPENDIX A: DETAILS OF THE FINITE DIFFERENCE OPERATORS

The expressions for the finite difference operators appearing in the Equations (11) and (20) are as follows:

$$\delta_x \phi_{ij} = \frac{\phi_{i+1,j} - \phi_{i-1,j}}{2h} \tag{A1}$$

$$\delta_y \phi_{ij} = \frac{\phi_{i,j+1} - \phi_{i,j-1}}{2k} \tag{A2}$$

$$\delta_x^2 \phi_{ij} = \frac{1}{h}\left\{\frac{\phi_{i+1,j}}{x_\mathrm{f}} - \left(\frac{1}{x_\mathrm{f}} + \frac{1}{x_\mathrm{b}}\right)\phi_{ij} + \frac{\phi_{i-1,j}}{x_\mathrm{b}}\right\} \tag{A3}$$

$$\delta_y^2 \phi_{ij} = \frac{1}{k}\left\{\frac{\phi_{i,j+1}}{y_\mathrm{f}} - \left(\frac{1}{y_\mathrm{f}} + \frac{1}{y_\mathrm{b}}\right)\phi_{ij} + \frac{\phi_{i,j-1}}{y_\mathrm{b}}\right\} \tag{A4}$$

$$\delta_x\delta_y\phi_{ij} = \frac{1}{4hk}\left(\phi_{i+1,j+1} - \phi_{i+1,j-1} - \phi_{i-1,j+1} + \phi_{i-1,j-1}\right) \tag{A5}$$

$$\delta_x\delta_y^2\phi_{ij} = \frac{1}{2hk}\left\{\frac{1}{y_f}\left(\phi_{i+1,j+1} - \phi_{i-1,j+1}\right) - \left(\frac{1}{y_f} + \frac{1}{y_b}\right)\left(\phi_{i+1,j} - \phi_{i-1,j}\right) + \frac{1}{y_b}\left(\phi_{i+1,j-1} - \phi_{i-1,j-1}\right)\right\} \tag{A6}$$

$$\delta_x^2\delta_y\phi_{ij} = \frac{1}{2hk}\left\{\frac{1}{x_f}\left(\phi_{i+1,j+1} - \phi_{i+1,j-1}\right) - \left(\frac{1}{x_f} + \frac{1}{x_b}\right)\left(\phi_{i,j+1} - \phi_{i,j-1}\right) + \frac{1}{x_b}\left(\phi_{i-1,j+1} - \phi_{i-1,j-1}\right)\right\} \tag{A7}$$

$$\begin{aligned}\delta_x^2\delta_y^2\phi_{ij} = \frac{1}{hk}\Bigg\{&\frac{\phi_{i+1,j+1}}{x_f y_f} + \frac{\phi_{i-1,j+1}}{x_b y_f} - \left(\frac{1}{x_f y_f} + \frac{1}{x_b y_f}\right)\phi_{i,j+1} - \left(\frac{1}{x_f y_f} + \frac{1}{x_f y_b}\right)\phi_{i+1,j}\\ &+ \left(\frac{1}{x_f y_f} + \frac{1}{x_f y_b} + \frac{1}{x_b y_f} + \frac{1}{x_b y_b}\right)\phi_{ij}\\ &- \left(\frac{1}{x_f y_b} + \frac{1}{x_b y_b}\right)\phi_{i,j-1} - \left(\frac{1}{x_b y_f} + \frac{1}{x_b y_b}\right)\phi_{i-1,j}\\ &+ \frac{\phi_{i+1,j-1}}{x_f y_b} + \frac{\phi_{i-1,j-1}}{x_b y_b}\Bigg\}\end{aligned} \tag{A8}$$

where x_f, x_b, y_f and y_b are defined in Section 2 and $h = (x_f + x_b)/2$ and $k = (y_f + y_b)/2$.

ACKNOWLEDGEMENTS

The first author would like to thank Professor M. M. Gupta, Department of Mathematics, The George Washington University, Washington DC for his valuable comments during the course of revision of the paper.

REFERENCES

1. Anderson DA, Tannehil JC, Pletcher RH. *Computational Fluid Mechanics and Heat Transfer*. Hemisphere Publishing Corporation: New York, 1984.
2. Anderson Jr JD. *Computational Fluid Dynamics*. McGraw-Hill, Inc.: New York, 1995.
3. Hoffman JD. *Numerical Methods for Engineers and Scientists*. McGraw-Hill, Inc.: Singapore, 1993.
4. Noye BJ, Tan HH. Finite difference methods for solving two-dimensional advection diffusion equation. *International Journal for Numerical Methods in Fluids* 1989; **9**:75–98.
5. Spotz WF, Carey GF. High-order compact scheme for the steady stream-function vorticity equations. *International Journal for Numerical Methods in Engineering* 1995; **38**:3497–3512.
6. Mackinnon RJ, Johnson RW. Differential equation based representation of truncation errors for accurate numerical solution. *International Journal for Numerical Methods in Fluids* 1991; **13**:739–757.
7. Strikwerda JC. High-order accurate schemes for incompressible viscous flow. *International Journal for Numerical Methods in Fluids* 1997; **24**:715–734.

8. Yanwen M, Dexun F, Kobayashi T, Taniguchi N. Numerical solution of the incompressible Navier–Stokes equations with an upwind compact difference scheme. *International Journal for Numerical Methods in Fluids* 1999; **30**:509–521.
9. Kalita JC, Dalal DC, Dass AK. A class of higher order compact schemes for the unsteady two-dimensional convection–diffusion equations with variable convection coefficients. *International Journal for Numerical Methods in Fluids* 2002; **38**:1111–1131.
10. Kalita JC. HOC schemes for incompressible viscous flows: application and development. *PhD Thesis*, Indian Institute of Technology Guwahati, May, 2002.
11. Li M, Tang T, Fornberg B. A compact fourth-order finite difference scheme for the steady incompressible Navier–Stokes equations. *International Journal for Numerical Methods in Fluids* 1995; **20**:1137–1151.
12. Gupta MM. High accuracy solutions of incompressible Navier–Stokes equations. *Journal of Computational Physics* 1991; **93**:343–359.
13. Kalita JC, Dalal DC, Dass AK. Fully compact higher order computation of steady state natural convection in a square cavity. *Physical Review E* 2001; **64**(6):066703 (1–13).
14. Spotz WF, Carey GF. Formulation and experiments with high-order compact schemes for nonuniform grids. *International Journal for Numerical Methods in Heat and Fluid Flow* 1998; **8**(3):288–303.
15. Zhang J, Lixin GE, Gupta MM. Fourth order compact difference scheme for 3D convection–diffusion equation with boundary layers on nonuniform grids. *Neural*, *Parallel and Scientific Computing* 2000; **8**:373–392.
16. Sleijpen GLG, van der Vorst HA. Hybrid bi-conjugate gradient methods for CFD problems. In *Computational Fluid Dynamics Review*, Hafez M, Oshima K (eds). Wiley: Chichester, 1995; 457–476.
17. Gartland Jr EC. Discrete weighted mean approximation of a model convection–diffusion equation. *SIAM Journal on Scientific and Statistical Computing* 1995; **3**:460–472.
18. Gupta MM, Manohar RM, Stephenson JH. A single cell high order scheme for the convection–diffusion equation with variable coefficients. *International Journal for Numerical Methods in Fluids* 1984; **4**:641–651.
19. Janssen RJA, Henkes RAWM. Accuracy of finite volume discretizations for bifurcating natural convection in a square cavity. *Numerical Heat Transfer* 1993; **24**:191–207.
20. Ghia U, Ghia KN, Shin CT. High-Re solutions for incompressible flow using the Navier–Stokes equation and a multigrid method. *Journal of Computational Physics* 1982; **48**:387–411.
21. Kim J, Moin P. Application of fractional step method to incompressible Navier–Stokes equations. *Journal of Computational Physics* 1985; **59**:308–323.
22. Schreiber R, Keller HB. Driven cavity flow by efficient numerical techniques. *Journal of Computational Physics* 1983; **49**:310–333.
23. Bruneau C-H, Jouron C. An efficient scheme for solving steady incompressible Navier–Stokes equations. *Journal of Computational Physics* 1990; **89**:389–413.

